Journal of Solid State Chemistry 210 (2014) 188–194

Contents lists available at ScienceDirect

Journal of Solid State Chemistry

journal homepage: www.elsevier.com/locate/jssc

Synthesis, structure and properties of the oxychalcogenide series $A_4O_4TiSe_4$ (A=Sm, Gd, Tb, Dy, Ho, Er and Y)

A.J. Tuxworth, J.S.O. Evans *

Department of Chemistry, Durham University, South Road, Durham DH1 3LE, United Kingdom

ARTICLE INFO

Article history:
Received 9 August 2013
Received in revised form
24 October 2013
Accepted 2 November 2013
Available online 21 November 2013

Keywords:
Synthesis
Oxychalcogenides
Rietveld refinement
Crystal structure
Electrical conductivity
Magnetic susceptibility

ABSTRACT

Seven oxyselenide materials have been synthesised with composition $A_4O_4TiSe_4$ (A=Sm, Gd–Er, Y) via solid state reactions of A_2O_3, $TiSe_2$ and Se at 900 °C. They are all isostructural with $Gd_4O_4TiSe_4$. Structures have been refined from powder X-ray diffraction data and have monoclinic $C2/m$ symmetry with unit cell parameters of $a \approx 15.7$ Å, $b \approx 3.75$ Å, $c \approx 9.65$ Å and $\beta \approx 117.5°$. They contain infinite ribbons of edge-sharing A_4O and A_3TiO tetrahedra 4 units wide, which are linked by chains of $TiSe_4O_2$ edge-sharing octahedra. Compositions A=Gd–Ho, Y are semiconductors with conductivities 1–3 Sm^{-1} at 300 K, with electronic band gaps of between 0.25 and 0.37 eV. Magnetic susceptibility is reported from 1.8 K to 300 K for compositions A=Gd–Ho. Rare earth moments appear to order antiferromagnetically at low temperatures with Gd and Tb showing evidence of ferromagnetism due to spin canting over a narrow temperature range close to T_N.

1. Introduction

Since the discovery of high temperature superconductivity in the layered AOFeAs (A=rare earth) oxypnictide systems there has been significant interest in mixed anion materials containing an oxide and a second anion [1–5]. LaOFeAs adopts the ZrCuSiAs structure and can be described as containing alternating layers of fluorite-like edge-shared La_4O tetrahedra and antifluorite-like edge-shared $FeAs_4$ tetrahedra. The A site is in a ASe_4O_4 4+4 distorted square antiprismatic coordination environment and links the two layers together. On changing the anion in the antifluorite layer from group 15 to group 16 (i.e. As^{3-} to Se^{2-}) charge balance requires 50% occupancy of the transition metal site, corresponding to a composition $AOFe_{0.5}Se$ or $A_2O_2FeSe_2$ (or $[AOSe]_2M$). Two basic structure types have been reported for this composition. α-$Ce_2O_2FeSe_2$ adopts a structure directly related to LaOFeAs where half of the tetrahedral sites in the antifluorite layers are occupied in an ordered arrangement, giving stripes of edge-shared tetrahedra of $[FeSe_2]^{2-}$ composition [6]. Other 2^+ metals (Mn, Zn, Cd) adopt different intralayer ordering patterns [7–9]. Alternatively $A_2O_2FeSe_2$ can adopt a different structural type, the β form, in which the fluorite-like rare earth oxide 2D layers are split into infinite ribbons four tetrahedra in width [10]. Fe is then found in a mixture of $FeSe_4$ tetrahedral sites and $FeSe_4O_2$ octahedral coordination environments.

In this paper we focus on the n=4 member of the $[AOSe]_nM$ series, whose structure has strong similarities to β-$La_2O_2FeSe_2$. The only known member of this family is $Gd_4O_4TiSe_4$. Single crystals of this phase, along with its crystal structure and magnetic properties were originally reported by Meerschaut et al. [11]. The structure contains fluorite-like ribbons four tetrahedra in width, linked by chains of edge-shared $TiSe_4O_2$ octahedra (Fig. 1). The α-, β-$A_2O_2FeSe_2$ and $Gd_4O_4TiSe_4$ structures thus form a series containing exclusively MSe_4 tetrahedra (M=transition metal) to mixed MSe_4O_2 octahedra and MSe_4 tetrahedra to exclusively MSe_4O_2 octahedra. As part of a study of the role of $[A_2O_2]^{2+}$ edge sharing tetrahedral units in stabilising mixed anion crystal structures we report the synthesis of bulk polycrystalline samples of $A_4O_4TiSe_4$ (A=Sm, Gd, Tb, Dy, Ho, Er and Y) for the first time and report their structures, electronic and magnetic properties. Ti containing oxyselenides are relatively rare. Previously reported examples include $A_{3.67}O_3Ti_2Se_6$ (A=Ce, Nd, Sm), $La_4O_4Ti_2Se_5$, $La_6O_5Ti_3Se_9$ and $Gd_4O_4TiSe_4$, all of which contain chains of $TiSe_4O_2$ distorted edge-sharing octahedra connecting rare-earth oxide units[11–13]. $A_3O_8Ti_3Se_2$ (A=Sm, Nd) is a more oxygen rich composition and contains TiO_6 and TiO_5Se octahedra [14,15].

2. Experimental

Polycrystalline samples of $A_4O_4TiSe_4$ (A=Sm, Gd–Er and Y) were prepared by the reaction of A_2O_3 (all >99.9% purity and heated to ~1000 °C prior to use), $TiSe_2$, synthesised from the

* Corresponding author. Tel.: +44 191 334 2093; fax: +44 191 384 4737.
E-mail address: john.evans@durham.ac.uk (J.S.O. Evans).

http://dx.doi.org/10.1016/j.jssc.2013.11.006
0022-4596

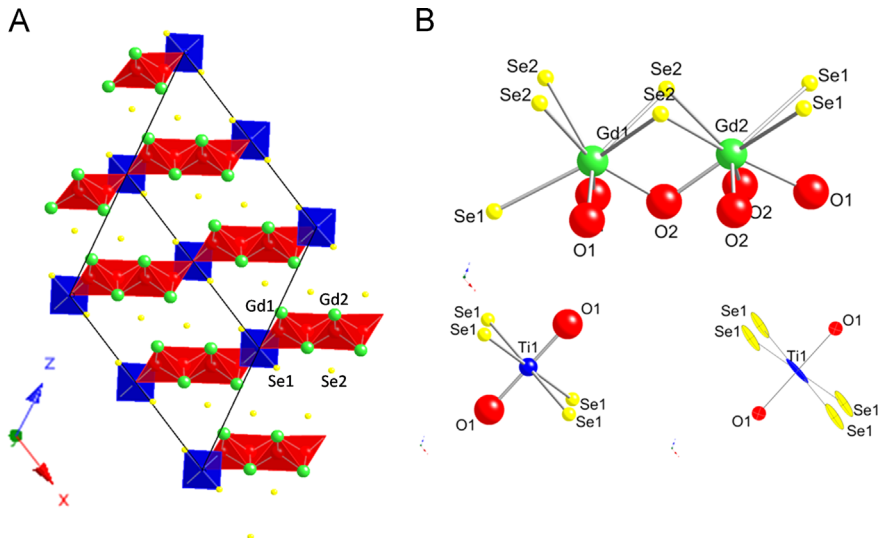

Fig. 1. (A) Illustration of the $A_4O_4TiSe_4$ crystal structure ($C2/m$ symmetry), A_4O and A_3TiO edge sharing tetrahedral ribbons in red, chains of edge-sharing $TiSe_4O_2$ in blue. (B) Coordination environments of selected atoms, including anisotropic thermal parameters for $TiSe_4O_2$ octahedra as reported for $Gd_4O_4TiSe_4$ by Meerschaut et al. [11]. Rare earth=green, titanium=blue, selenium=yellow, and oxygen=red. (For interpretation of the references to colour in this figure caption, the reader is referred to the web version of this article.)

reaction of Ti (99.999%, British Dry Houses Ltd) and Se (99.999%, Alfa Aesar) powders at 800 °C, and Se powders in a 2:1:2 ratio. Reagents were intimately ground together using an agate pestle and mortar and placed inside a 7 mm diameter high density alumina crucible. 325-mesh Al powder (10% molar excess relative to the stoichiometric amount) was placed in a separate alumina crucible to act as an oxygen getter (forming Al_2O_3 during the reaction). The overall reaction is $2A_2O_3+TiSe_2+2Se+{}^4/_3Al \rightarrow A_4O_4TiSe_4+{}^2/_3Al_2O_3$. The two crucibles were sealed inside evacuated quartz ampoules and heated with the following routine: ramp to 600 °C at 5 °C min^{-1} and dwell 12 h, ramp to 800 °C at 0.5 °C min^{-1}, dwell 1 h, ramp to 900 °C at 1 °C min^{-1}, and dwell 72 h. The furnace was then allowed to cool to room temperature. All products were produced as black powders; analysis of the products by powder X-ray diffraction confirmed the target phase had been obtained, and that all Al had been oxidised to Al_2O_3. Under these reaction conditions it was not possible to synthesise the Nd, Eu or Yb analogues, with ternary oxychalcogenides phases being formed.

X-ray powder diffraction (XRPD) data were collected using Bruker D8 Advance diffractometers (reflection mode, Cu$K\alpha_1/K\alpha_2$ radiation, Lynxeye Si strip detector, step size 0.02°, variable divergence slits) equipped with either a sample changer or an Oxford Cryosystems PheniX cryostat. Samples were sprinkled onto a zero-background Si wafer and held in place with a thin layer of Vaseline. Data were collected over a period of 12 h at room temperature from 5° to 120° 2θ. Twenty minute scans were also collected at 5 K intervals on cooling and warming between 12 and 300 K. Powder diffraction data were analysed by the Rietveld method [16] using the TOPAS Academic (TA) software suite controlled via local routines [17,18]. Short data collections were analysed to determine the temperature dependence of lattice parameters, while structural refinements were performed using long data collections. The background (Chebyshev polynomial), sample height, peak shapes (pseudo-Voigt), unit cell parameters, atomic positions (oxygens fixed), isotropic thermal parameters, phase fractions and cell parameters of minor impurity content were also typically refined.

Magnetic measurements were carried out using a Quantum Design SQUID magnetometer in the temperature range 2–292 K. Four-probe measurements of conductivity were carried out using a Quantum Design Physical Properties Measurement System (PPMS) with copper electrodes attached to rectangular (volume ~70 mm^3) pellets using silver paste.

3. Results and discussion

3.1. Structure

In this work we have prepared a bulk polycrystalline sample of $Gd_4O_4TiSe_4$ for the first time along with six new $A_4O_4TiSe_4$ (A=Sm, Gd–Er and Y) analogues, summarised in Table 1. For A=Gd to Ho and Y essentially phase pure samples (impurities $<1\%$ by weight) could be prepared. For Sm, the largest rare earth phase accessible, the highest phase purity obtained was ~90 wt.%; for the smallest rare earth, Er, purity was ~75%. We could not prepare larger or smaller rare earth analogues under these conditions. The seven compounds are all isostructural and adopt the $C2/m$ monoclinic structure reported by Meerschaut et al. for $Gd_4O_4TiSe_4$ [11]. Plots of Rietveld refinements confirming the structure and phase purity are included in supplementary information along with refined metal and Se fractional coordinates. Cell parameters for each phase are included in Table 1. Fig. 2 shows that there is an essentially smooth increase in cell parameters and unit cell volume with A site ionic radius.

The structure of $A_4O_4TiSe_4$ materials is shown in Fig. 1, it has some similarities to the LaOFeAs structure with oxide and chalcogenide ions segregated into layers, though these are zig–zag in nature due to the infinite fluorite A_4O layers being interrupted by Ti sites. Oxide ions are found in infinite ribbons of four edge-sharing tetrahedra which run parallel to the b-axis and contain A_4O and A_3TiO oxygen coordination environments. There are two crystallographically independent A^{3+} ions which have either ASe_4O_4 or ASe_5O_3 4+4 square antiprismatic coordination environments. The ASe_4O_4 square antiprism of $A2$ is similar to that found in LaOFeAs phases, though with small distortion due to the loss of 4-fold symmetry. The finite width of the tetrahedral ribbons means that one oxygen is replaced by selenium around the $A1$ site forming ASe_5O_3 units. The tetrahedral ribbons are interconnected by $TiSe_4O_2$ octahedra which themselves form edge-shared chains parallel to the b-axis. The Se sites in the $TiSe_4O_2$ octahedra form part of the $A1$ ASe_5O_3 coordination polyhedra, whilst the O sites are those ($O1$) at the edge of the tetrahedral ribbons with A_3TiO pseudo-tetrahedral coordination. Work by Meerschaut et al. on the only phase previously reported, $Gd_4O_4TiSe_4$, shows the U_{22} parameter for Ti is much higher than for other atoms while the U_{33} parameter is especially low, as shown in Fig. 1b [11].

Table 1
Unit cell parameters from Rietveld analysis of XRPD data in space group $C2/m$ for $A_4O_4TiSe_4$ at 295 and 12 K. Numbers in parentheses are Rietveld-derived standard uncertainties.

	$Sm_4O_4TiSe_4$	$Gd_4O_4TiSe_4$	$Tb_4O_4TiSe_4$	$Dy_4O_4TiSe_4$	$Ho_4O_4TiSe_4$	$Er_4O_4TiSe_4$	$Y_4O_4TiSe_4$
a (Å)							
295 K	15.8920(2)	15.7901(3)	15.6791(3)	15.5962(2)	15.5577(2)	15.4992(4)	15.5693(2)
12 K	15.8601(3)	15.7809(3)	15.6581(3)	15.5636(3)	15.5259(2)	–	15.5541(1)
b (Å)							
295 K	3.79668(4)	3.75792(5)	3.74085(7)	3.71985(4)	3.70315(4)	3.68819(7)	3.71079(4)
12 K	3.78966(5)	3.74887(5)	3.73413(6)	3.71383(5)	3.69456(4)	–	3.70168(4)
c (Å)							
295 K	9.7088(1)	9.6641(1)	9.6179(2)	9.5886(1)	9.5686(1)	9.5449(2)	9.5911(1)
12 K	9.6800(2)	9.6462(2)	9.5883(2)	9.5682(2)	9.5485(1)	–	9.5702(1)
Beta (°)							
295 K	117.5170(9)	117.672(1)	117.544(1)	117.532(1)	117.6000(9)	117.556(2)	117.5407(9)
12 K	117.493(1)	117.736(1)	117.507(1)	117.491(1)	117.6123(1)	–	117.578(1)
Volume (Å^3)							
295 K	519.53(1)	507.86(1)	500.18(2)	493.29(1)	488.54(1)	483.73(2)	491.33(1)
12 K	516.10(1)	505.10(1)	497.25(2)	490.59(2)	485.33(1)	–	488.41(1)

3.2. Thermal expansion

Powder diffraction patterns of six of these compositions (A=Sm, Gd–Ho, and Y) were recorded as a function of temperature from 300 to 12 K. No additional reflections or peak splittings were observed on cooling to indicate any major structural phase changes. Fig. 3 shows the evolution of the unit cell volumes obtained from Rietveld refinement. For the smaller A site elements Tb–Ho and Y a smooth variation in unit cell volume was observed. The overall volume expansion of each phase was similar, with a volume of coefficient of thermal expansion $\alpha_V = V_{T1} - V_{T2}/V_{T1}(T2-T1)$ ranging from 2.1×10^{-5} to 2.3×10^{-5} K^{-1} over the temperature range 12–300 K. As shown in supplementary information, individual cell parameters showed slight differences in thermal expansion, this being most notable in the cell angle β which form two groups with positive and negative temperature gradients. The three materials (Gd, Ho, Y) for which β decreases with temperature have a larger linear expansion in the b cell parameter than other phases.

The behaviour of $Gd_4O_4TiSe_4$ and $Sm_4O_4TiSe_4$ below ~100 K differs from that of the other members of the series with a sharp increase in a cell parameter and a discontinuity in β on cooling (Fig. 4). a and β also show hysteretic behaviour, with values on warming differing from values on cooling. This behaviour is repeatable. Fig. 4 also contains the cell parameters of $Gd_4O_4TiSe_4$ when quench-cooled from 300 to 12 K in 42 min (the maximum cooling rate of the cryostat) and then held at this temperature for ~22 h. These data show that a and β change with time while the other unit cell parameters remained effectively unchanged. For A=Gd a increases from 15.7742(4) to 15.7802(5) Å, and β from 117.716(2)° to 117.737(2)°. Similar, but less pronounced, behaviour was observed for $Sm_4O_4TiSe_4$ (see supplementary information). No marked changes in either peak intensities or peak splitting were observed during this process for either phase.

The origins of this unusual behaviour are not clear, however, Meerschaut et al. report a large thermal parameter for Ti from single crystal studies [11]. This is consistent with the large isotropic thermal parameters for $Gd_4O_4TiSe_4$ obtained in this work. Meerschaut observed that the Ti U_{22} anisotropic thermal parameter is much higher than those of the other atoms, while the U_{33} is too low to be physically reasonable, suggesting that the Ti position could be displaced from (0,0,0). The ellipsoid shape suggests displacement in the ab plane (approximately the $TiSe_4$ plane) to an ($0,y,0$) or ($x,y,0$) position with x and y close to zero. It therefore seems likely that the discontinuities in unit cell parameters at low temperature could be caused by displacement of the Ti site from the centre of the $TiSe_4O_2$ octahedron at low temperature (either short or long range order). This idea is supported by the relatively low bond valence sum (3.5) at the Ti site. Off-centre Ti displacements have been observed in other $TiSe_4O_2$ octahedra [13]. Whilst our diffraction data give strong evidence from peak positions and cell parameters of a low temperature phase transition, peak intensity changes are not sufficient to determine its precise nature. We note that calculated X-ray diffraction patterns for Ti ordering at ($0,y,0$) with y=0.05 would lead to a maximum intensity of superstructure reflections of only ~0.1% of the most intense reflection.

3.3. Conductivity measurements

The conductivity of pelletised samples of $A_4O_4TiSe_4$ (A=Gd, Tb, Dy, Ho and Y) was measured on cooling and warming between 300 K and 130–70 K (depending on where the sample resistance became too high to measure). Room temperature conductivities are given in Table 2 and show an increase in conductivity with decreasing rare earth radius. Plots of ln(conductivity) vs reciprocal temperature show linear behaviour for all samples (Fig. 5), indicating semiconducting behaviour with activation energies of between ~0.19 and ~0.13 eV, suggesting electronic band gaps between 0.378(2) and 0.254(3) eV (Table 2). Preliminary DFT calculations suggest the top of the valence band has predominantly Se p character and the bottom of the conduction band predominantly Ti d character. The smooth decrease in band gap presumably arises from band broadening as the rare earth radius and unit cell volume decreases.

3.4. Magnetic measurements

Magnetic properties of A=Gd, Tb, Dy and Ho were measured in the temperature range 2–292 K with magnetic fields of 100 and 10 Oe. Magnetisation vs applied field plots at 292 K were linear for all four samples, with an essentially zero intercept indicating paramagnetic behaviour at this temperature with no significant ferromagnetic impurities. All samples showed a linear variation of $1/\chi$ vs temperature at high temperature, which were fitted using the Curie–Weiss law. The negative values of the Weiss constants (Table 3), indicate weak antiferromagnetic interactions in all four compounds. All samples showed effective magnetic moments deduced from the Curie constants (32–292 K) close to the expected Landé values for A^{3+} ions, which is consistent with the presence of Ti^{4+}.

Fig. 6a shows $Gd_4O_4TiSe_4$ field cooled (FC) and zero field cooled (ZFC) data collected in 5 K intervals with more closely spaced FC

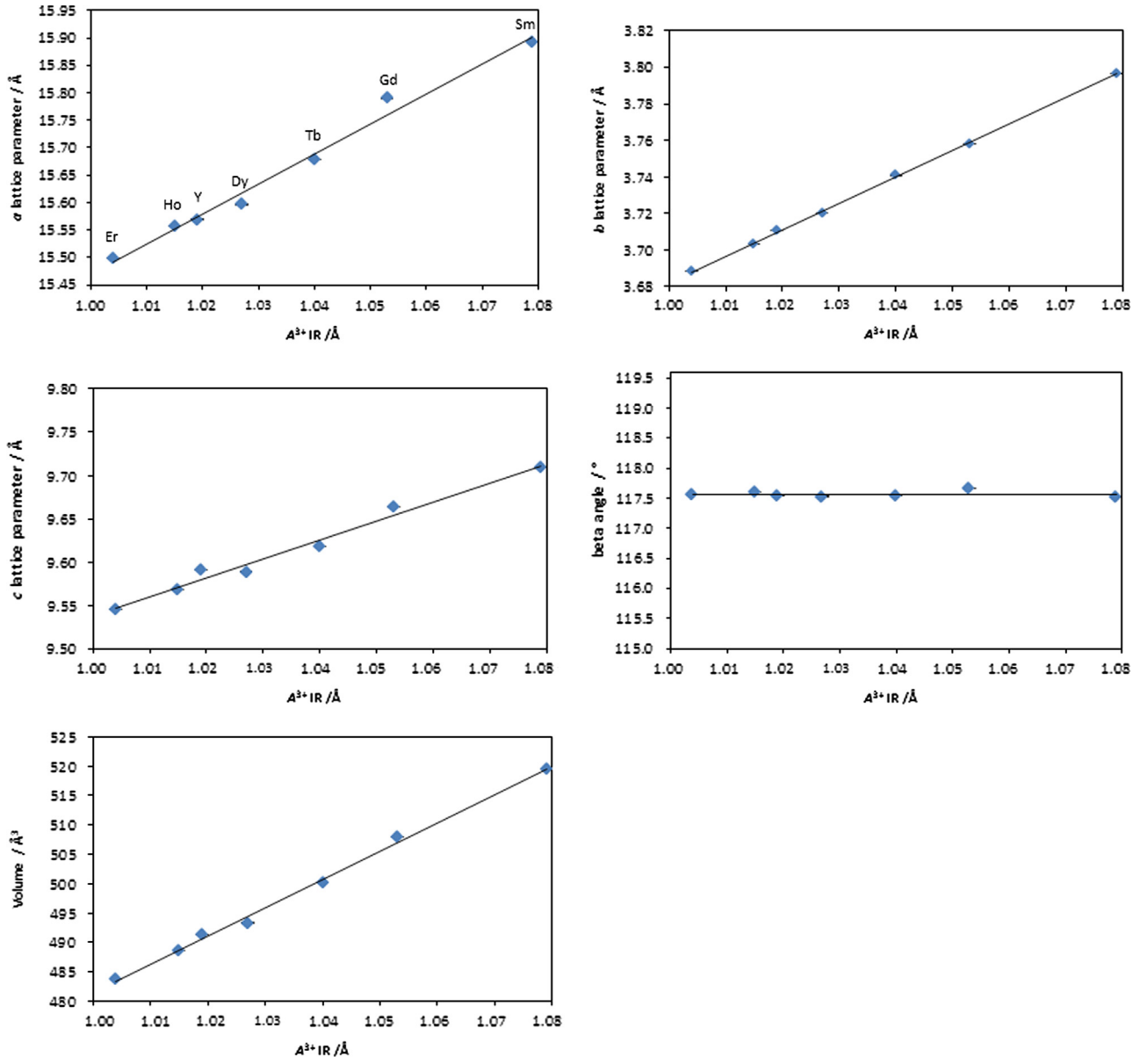

Fig. 2. The effect of increasing rare-earth radius on the unit cell parameters of $A_4O_4TiSe_4$, error bars contained within the data points.

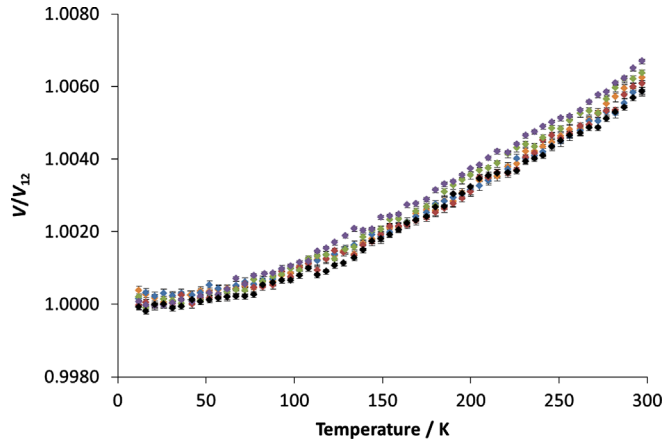

Fig. 3. Unit cell volumes of $A_4O_4TiSe_4$ (A= Sm, Gd–Ho) as a function of temperature between 300 and 12 K, obtained from refinement of XRPD data. $Sm_4O_4TiSe_4$=orange, $Gd_4O_4TiSe_4$=blue, $Tb_4O_4TiSe_4$=red, $Dy_4O_4TiSe_4$=green, $Ho_4O_4TiSe_4$=purple, $Y_4O_4TiSe_4$=black. (For interpretation of the references to colour in this figure caption, the reader is referred to the web version of this article.)

measurements taken between 2 and 10 K; no difference in FC and ZFC measurements was observed. The μ_{calc} and θ values for $Gd_4O_4TiSe_4$ are similar to those reported by Meerschaut et al. of μ_{calc} 7.94 μ_B/Gd and θ −12.8(2) K [11]. A sharp increase in susceptibility is observed between 2.5 and 4 K, which is in agreement with data reported by Meerschaut et al. [11]. Fig. 6b shows the field dependence of this feature in susceptibility for our sample. We observe a ~1.5-fold increase in peak susceptibility between 100 and 10 Oe compared to the ~4-fold increase reported by Meerschaut. The overall behaviour has been attributed [11] to a transition to an antiferromagnetically ordered state below ~1.5 K. Between ~4 and 2.5 K a small canting of the Gd spins (approximately 3°) is suggested to give a ferromagnetic component to the susceptibility which disappears at low temperature. This canting saturates at relatively low field (a few hundred Oe) giving rise to the observed field-dependent susceptibility below the saturation field.

Fig. 7a shows FC and ZFC susceptibility data for $Tb_4O_4TiSe_4$ between 2 and 300 K measured at 100 Oe, and Fig. 7b compares data measured in fields of 10 and 100 Oe. In contrast to $Gd_4O_4TiSe_4$ there is no marked increase in susceptibility on cooling. Both FC

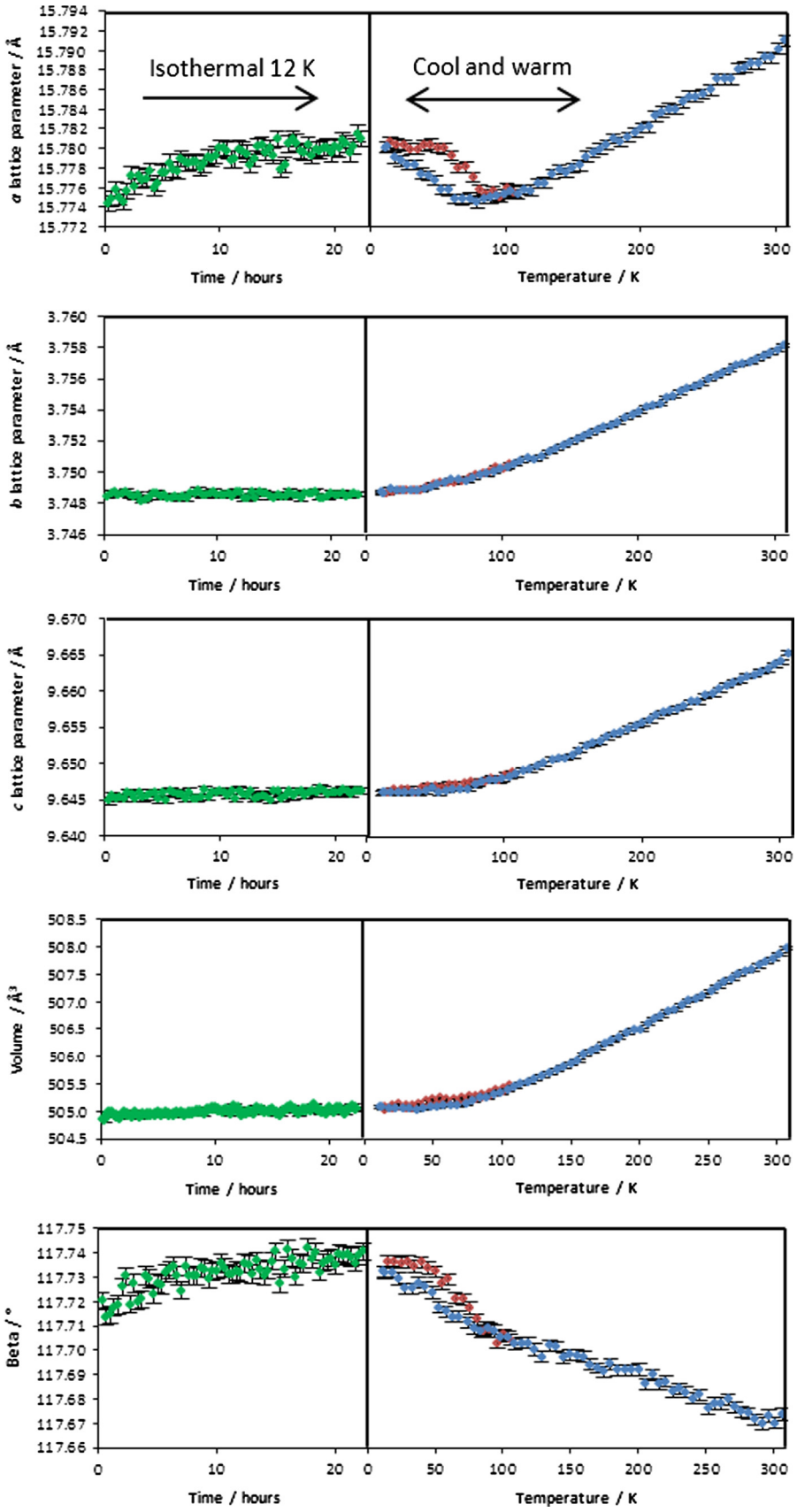

Fig. 4. Unit cell parameters of $Gd_4O_4TiSe_4$ extracted from XRPD data collected at 12 K following rapid cooling (green, left), and on cooling (blue, filled) and warming (red, open) at 5 K h^{-1}. (For interpretation of the references to colour in this figure caption, the reader is referred to the web version of this article.)

and ZFC data recorded at 100 Oe show a decrease in susceptibility below 4 K suggesting antiferromagnetic ordering. The upturn in susceptibility at ~5 K and the field dependence of susceptibility could indicate a small ferromagnetic component due to canting as in $Gd_4O_4TiSe_4$. The magnitude of any canting is, however, significantly lower than in the Gd phase. The deviation between ZFC and FC curves at low temperature is presumably related to unblocking of local ferromagnetic domains at the relatively low measurement field.

Table 2
Room temperature conductivities and electronic band gaps for $A_4O_4TiSe_4$ (A=Gd, Tb, Dy, Ho and Y) series.

Compound	Room temperature conductivity (Sm^{-1})	Band gap (eV)
$Gd_4O_4TiSe_4$	1.04	0.378(2)
$Tb_4O_4TiSe_4$	1.02	0.331(2)
$Dy_4O_4TiSe_4$	1.85	0.307(3)
$Ho_4O_4TiSe_4$	2.90	0.254(3)
$Y_4O_4TiSe_4$	1.68	0.317(3)

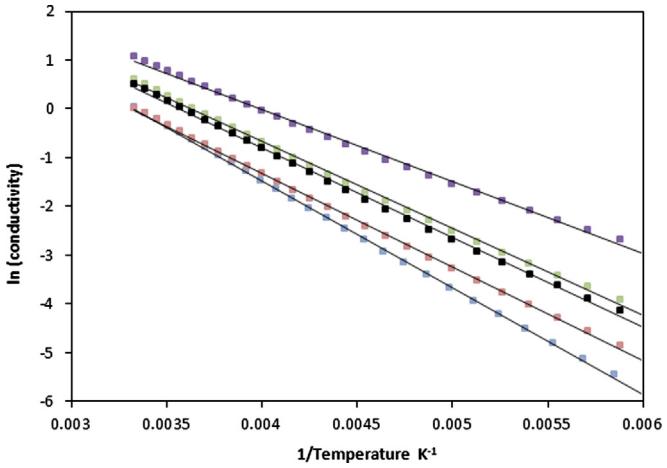

Fig. 5. Temperature dependence of conductivity for $Gd_4O_4TiSe_4$ (blue), $Tb_4O_4TiSe_4$ (red), $Dy_4O_4TiSe_4$ (green), $Ho_4O_4TiSe_4$ (purple) and $Y_4O_4TiSe_4$ (black). (For interpretation of the references to colour in this figure caption, the reader is referred to the web version of this article.)

Table 3
Experimental magnetic moments μ_{calc} and Weiss constants (θ) obtained from fitting 100 Oe FC data in the range 32–292 K.

Compound	μ_{calc} (μ_B/A)	μ_{eff} (μ_B/A)	θ (K)
$Gd_4O_4TiSe_4$	7.82(1)	7.94	−5.6(5)
$Tb_4O_4TiSe_4$	9.26(2)	9.72	−9.6(8)
$Dy_4O_4TiSe_4$	10.28(1)	10.65	−5.3(4)
$Ho_4O_4TiSe_4$	10.36(1)	10.60	−4.6(3)

Fig. 8 shows data for $Dy_4O_4TiSe_4$ and $Ho_4O_4TiSe_4$ which suggest antiferromagnetic ordering with $T_N \approx 4$ K with no increase in susceptibility prior to or following this transition. The rare earth ordering temperatures observed for these phases are comparable to those of, for example $AFeO_3$ materials. In $GdFeO_3$ a maximum is susceptibility at 2.5 K is attributed to antiferromagnetic ordering of the Gd moments, while in $TbFeO_3$ system there is some interaction between the Fe and Tb spin below 10 K, with Tb moments ordering antiferromagnetically below 3.1 K [19–21]. In $DyFeO_3$ ordering occurs below 4.5 K and $HoFeO_3$ is reported to have a T_N of 4.1 K [22]. In each of these systems the Fe sites order antiferromagnetically with Néel temperatures in excess of 600 K [23,24].

4. Conclusions

We describe here the synthesis of bulk polycrystalline samples of six new members of the $A_4O_4TiSe_4$ family of materials. Synthesis of other rare-earth containing materials was unsuccessful, suggesting that the structure is only accessible using this synthetic route for rare earths with resulting cell volumes ranging from ~483 to 520 $Å^3$. Variable temperature X-ray diffraction experiments shows the Sm and Gd analogues undergo a structural distortion on cooling, revealed most clearly in the a lattice parameter and monoclinic angle β. We presume this is an order disorder transition associated with off-centre distortion of the $TiSe_4O_2$ octahedra. Conductivity measurements show the series to be semiconductors, with electronic band gaps of between 0.378 (2) and 0.254(3) eV. SQUID magnetometry shows that $Gd_4O_4TiSe_4$ has a significant increase in susceptibility between 2.5 and 4 K consistent with previous measurements, which is presumed to be due to spin canting prior to the onset of full antiferromagnetic order. $Tb_4O_4TiSe_4$ shows similar but less pronounced effects. $Dy_4O_4TiSe_4$ and $Ho_4O_4TiSe_4$ order antiferromagnetically below 4 K.

Acknowledgments

We are grateful to EPSRC for funding and Dr R. Coleman for assistance with SQUID measurements.

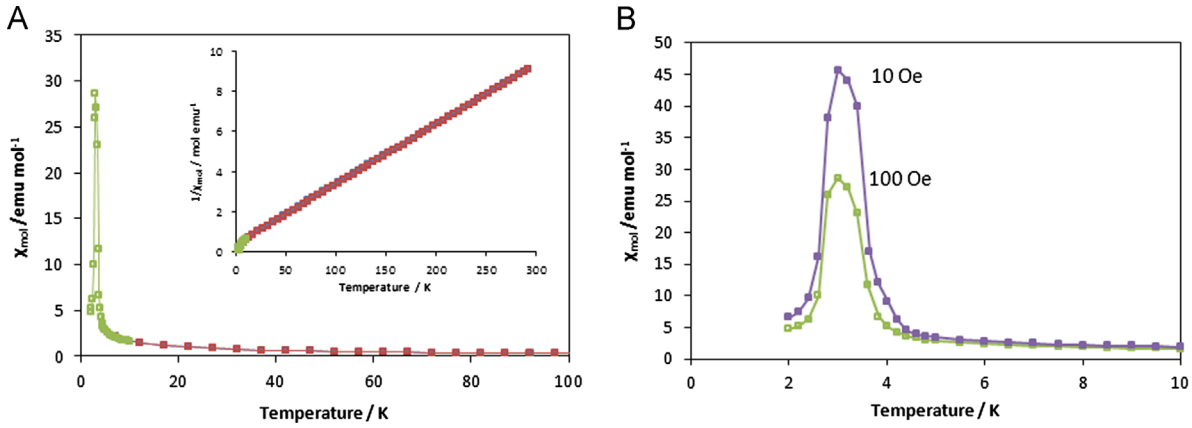

Fig. 6. (A) Magnetic susceptibility and inverse susceptibility (inset) of $Gd_4O_4TiSe_4$ at 100 Oe, a sharp increase in susceptibility is observed between 4 and 2.5 K. (B) Field dependence of susceptibility peak. FC=red (open), ZFC=blue (closed), additional FC data points=green (open), 10 Oe FC=purple (closed). (For interpretation of the references to colour in this figure caption, the reader is referred to the web version of this article.)

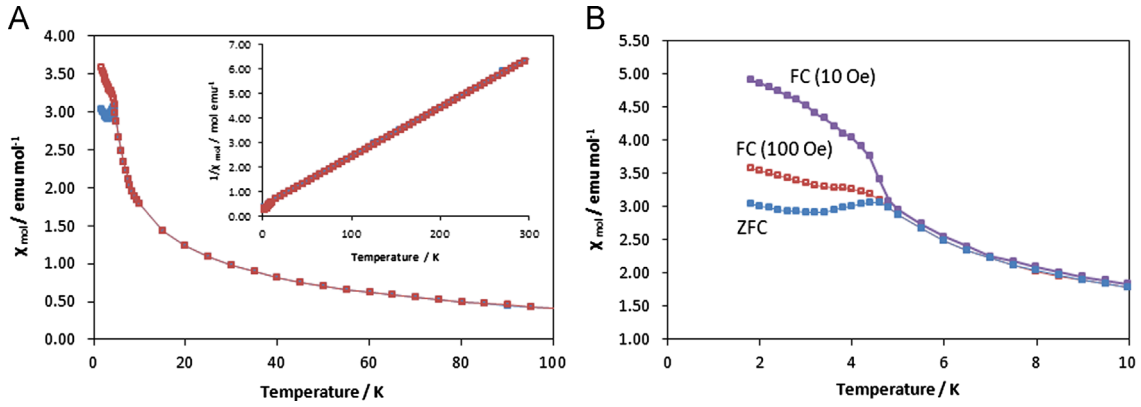

Fig. 7. (A) Magnetic susceptibility and inverse susceptibility (inset) of $Tb_4O_4TiSe_4$ vs temperature under an applied field of 100 Oe. (B) Susceptibility between 2 and 10 K. 100 Oe FC= red (open), ZFC=blue (closed); 10 Oe FC=purple (closed). (For interpretation of the references to colour in this figure caption, the reader is referred to the web version of this article.)

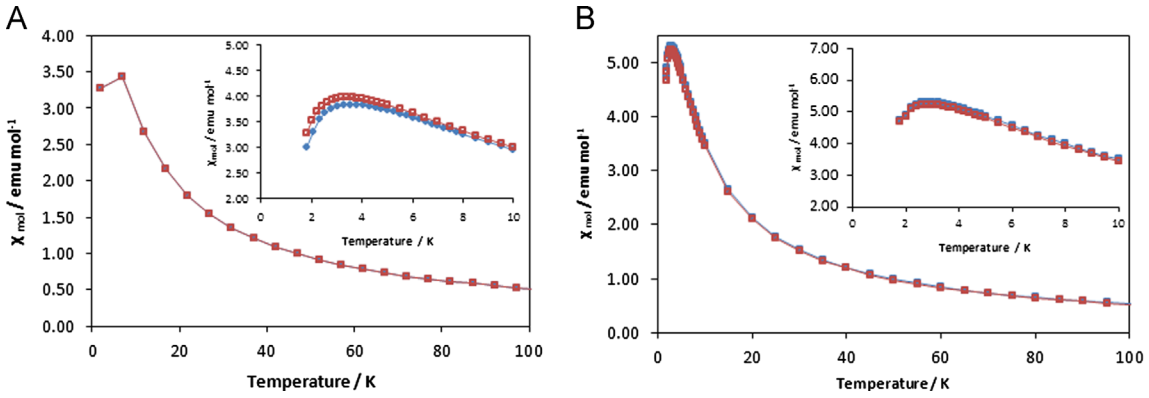

Fig. 8. FC and ZFC Magnetic susceptibility of (A) $Dy_4O_4TiSe_4$ and (B) $Ho_4O_4TiSe_4$ at 100 Oe, insets low temperature regions. FC =red (open), ZFC =blue (closed). (For interpretation of the references to colour in this figure caption, the reader is referred to the web version of this article.)

Appendix A. Supporting information

Supplementary data associated with this article can be found in the online version at http://dx.doi.org/10.1016/j.jssc.2013.11.006.

References

[1] Y. Kamihara, T. Watanabe, M. Hirano, H. Hosono, J. Am. Chem. Soc. 130 (2008) 3296–3297.
[2] C. de la Cruz, Q. Huang, J.W. Lynn, J.Y. Li, W. Ratcliff, J.L. Zarestky, H.A. Mook, G. F. Chen, J.L. Luo, N.L. Wang, P.C. Dai, Nature 453 (2008) 899–902.
[3] J. Paglione, R.L. Greene, Nat. Phys. 6 (2010) 645–658.
[4] Y. Kamihara, H. Hiramatsu, M. Hirano, R. Kawamura, H. Yanagi, T. Kamiya, H. Hosono, J. Am. Chem. Soc. 128 (2006) 10012–10013.
[5] H.-H. Wen, G. Mu, L. Fang, H. Yang, X. Zhu, EPL 82 (2008).
[6] E.E. McCabe, D.G. Free, J.S.O. Evans, Chem. Commun., 47, 1261–1263.
[7] I. Ijjaali, K. Mitchell, C.L. Haynes, A.D. McFarland, R.P. Van Duyne, J.A. Ibers, J. Solid State Chem. 176 (2003) 170–174.
[8] A.J. Tuxworth, E.E. McCabe, D.G. Free, S.J. Clark, J.S.O. Evans, Inorg. Chem., 52, 2078–2085.
[9] H. Hiramatsu, K. Ueda, T. Kamiya, H. Ohta, M. Hirano, H. Hosono, J. Phys. Chem. B 108 (2004) 17344–17351.
[10] E.E. McCabe, D.G. Free, B.G. Mendis, J.S. Higgins, J.S.O Evans, Chem. Mater., 22, 6171–6182.
[11] A. Meerschaut, A. Lafond, V. Meignen, C. Deudon, J. Solid State Chem. 162 (2001) 182–187.
[12] O. Tougait, J.A. Ibers, Chem. Mater. 12 (2000) 2653–2658.
[13] O. Tougait, J.A. Ibers, J. Solid State Chem. 157 (2001) 289–295.
[14] V. Meignen, C. Deudon, A. Lafond, C. Boyer-Candalen, A. Meerschaut, Solid State Sci. 3 (2001) 189–194.
[15] H. Person, W. Urland, J. Alloys Compds. 323 (2001) 57–60.
[16] H.M. Rietveld, J. Appl. Crystallogr. 2 (1969) 65–71.
[17] A.A. Coelho, J. Appl. Crystallogr. 36 (2003) 86–95.
[18] A.A. Coelho, TOPAS Academic: General Profile and Structure Analysis Software for Powder Diffraction Data, 2012.
[19] Y. Tokunaga, N. Furukawa, H. Sakai, Y. Taguchi, T.-h. Arima, Y. Tokura, Nat. Mater. 8 (2009) 558–562.
[20] J. Tejada, X.X. Zhang, A. Roig, O. Nikolov, E. Molins, Europhys. Lett. 30 (1995) 227–232.
[21] J.D. Cashion, A.H. Cooke, D.M. Martin, M.R. Wells, J. Appl. Phys. 41 (1970) 1193–1194.
[22] I. Nowik, H.J. Williams, Physics Letters 20 (1966) 154–156.
[23] M. Shao, S. Cao, Y. Wang, S. Yuan, B. Kang, J. Zhang, Solid State Commun. 152 (2012) 947–950.
[24] A. Bhattacharjee, K. Saito, M. Sorai, J. Phys. Chem. Solids 63 (2002) 569–574.